

in Table I shows a smooth behavior, as expected from physics. This further validates our extraction method.

IV. CONCLUSION

A new procedure for extracting the intrinsic HBT equivalent-circuit parameters is presented, which allows for direct calculation of all elements. For the first time, a linear least-square estimation algorithm has been used to solve a set of equations, which evolves from S -parameter measurements at a large number of frequencies. In this way, the frequency dependence of several combinations of the intrinsic elements is utilized to extract each of these elements. The method is fast and provides unique solutions. It has been validated in the frequency range of 0.05–35 GHz.

ACKNOWLEDGMENT

The authors would like to thank the wafer processing groups of the Ferdinand-Braun-Institut für Höchstfrequenztechnik, Berlin, Germany, for providing the HBT's, S. Schulz for performing measurements, and Dr. W. Heinrich for helpful discussions and continuous encouragement.

REFERENCES

- [1] G. Dambrine, A. Cappy, F. Heliodore, and E. Playez, "A new method for determining the FET small-signal equivalent circuit," *IEEE Trans. Microwave Theory Tech.*, vol. 36, pp. 1151–1159, July 1988.
- [2] C.-J. Wei and J. C. M. Hwang, "Direct extraction of equivalent circuit parameters for heterojunction bipolar transistors," *IEEE Trans. Microwave Theory Tech.*, vol. 43, pp. 2035–2039, Sept. 1995.
- [3] Y. Gobert, P. J. Tasker, and K. H. Bachem, "A physical, yet simple, small-signal equivalent circuit for the heterojunction bipolar transistor," *IEEE Trans. Microwave Theory Tech.*, vol. 45, pp. 149–153, Jan. 1997.
- [4] D. Costa, W. Liu, and J. S. Harris, "Direct extraction of the Al-GaAs/GaAs heterojunction bipolar transistor small-signal equivalent circuit," *IEEE Trans. Electron Devices*, vol. 38, pp. 2018–2024, Sept. 1991.
- [5] S. Lee and A. Gopinath, "Parameter extraction technique for HBT equivalent circuit using cutoff mode measurement," *IEEE Trans. Microwave Theory Tech.*, vol. 40, pp. 574–577, Mar. 1992.
- [6] P. Heymann, R. Doerner, and F. Schnieder, "Determination of small-signal equivalent circuit elements and large-signal model parameters of Si/SiGe HBT's up to 50 GHz," in *IEEE Workshop Silicon-Based High-Frequency Devices and Circuits Dig.*, Günzburg, Germany, Nov. 10–11, 1994, pp. 90–96.
- [7] U. Schaper and B. Holzapfl, "Analytical parameter extraction of the HBT equivalent circuit with T-like topology from measured S -parameters," *IEEE Trans. Microwave Theory Tech.*, vol. 43, pp. 493–498, Mar. 1995.
- [8] D. Peters, W. Daumann, W. Brockerhoff, R. Reuter, E. Koenig, and F. J. Tegude, "Direct calculation of the HBT small-signal equivalent circuit with special emphasize to the feedback capacitance," in *European Microwave Conf. Dig.*, vol. 2, 1995, pp. 1032–1036.
- [9] C. Rheinfelder, M. Rudolph, F. Beißwanger, and W. Heinrich, "Non-linear modeling of SiGe HBT's up to 50 GHz," in *IEEE MTT-S Int. Microwave Symp. Dig.*, 1997, pp. 877–880.
- [10] S. A. Maas and D. Tait, "Parameter-extraction method for heterojunction bipolar transistors," *IEEE Microwave Guided Wave Lett.*, pp. 502–504, Dec. 1992.
- [11] J. W. Linnik, *Method of Least Squares and Principles of the Theory of Observations*. New York: Pergamon, 1961.
- [12] E. Richter, P. Kurpas, U. Zeimer, B. Janke, S. Hähle, K. Vogel, W. Weyers, and J. Würfl, "Optimization of GaInP/GaAs-HBT-structures by combination of material and device analysis," in *Proc. 20th WOCSDICE'96*, Vilnius, Lithuania, 1996.

Microwave Diversity Imaging Using Six-Port Reflectometer

Hsin-Chia Lu and Tah-Hsiung Chu

Abstract—A microwave diversity imaging system conventionally uses a vector network analyzer (VNA) to directly measure the object scattered field (amplitude and phase) over a selected frequency range and viewing angles, then reconstructs the scattering object characteristic function through two-dimensional Fourier inversion. In this paper, we present a cost-effective microwave diversity imaging system using a six-port reflectometer, which measures four amplitude (or power) values to acquire the object scattered field indirectly. One can then eliminate the coherent detectors in a VNA. The calibration procedure for this microwave diversity imaging measurement is also described. Experimental results of three types of scattering objects, a metallic cylinder, four distributed line scatterers, and a 72:1 scaled B-52 aircraft model, are presented using the described six-port microwave imaging system.

Index Terms—Microwave diversity imaging, six-port reflectometer.

I. INTRODUCTION

As a perfectly conducting convex object is illuminated with a monochromatic plane wave, under physical optics approximation, its range-normalized backscattered far field and the object characteristic function forms a Fourier transformation pair. This relationship is known as the Bojarski's identity [1], [2]. To effectively acquire more scattering information about the object in its Fourier domain, the frequency and angular diversity techniques are developed with the use of a vector network analyzer (VNA) [3]. After sufficient amount of data are measured and recorded accordingly in the Fourier domain, two-dimensional Fourier inversion then yields a microwave projection image of the scattering object.

A six-port reflectometer described in [4] and [5] is known as a low-cost and high-frequency alternate to a conventional VNA to measure the reflection coefficient of microwave devices. In this paper, we use a six-port reflectometer for microwave diversity imaging measurement in a compact-range arrangement and develop the associated calibration method. In the calibration, a reference object is placed at the object positioner with the use of a calibration circuit. Microwave diversity imaging experiments are conducted for three types of scattering objects, a metallic cylinder, four distributed line scatterers, and a scaled B-52 aircraft model. The operation frequency is from 8 to 12 GHz.

II. MICROWAVE DIVERSITY IMAGING AND SIX-PORT REFLECTOMETER

A. Microwave Diversity Imaging Technique

As a perfectly conducting convex object is illuminated by a monochromatic plane wave propagating in the direction of \mathbf{i}_k , its range-normalized backscattered far field, under physical optics approximation, can be expressed as [1], [2]

$$\frac{\rho(\mathbf{p})}{p} = \frac{j}{2\sqrt{\pi}} \int_{\mathbf{i}_p \cdot \mathbf{n} > 0} (\mathbf{i}_p \cdot \mathbf{n}) e^{-j\mathbf{p} \cdot \mathbf{r}} dS(\mathbf{r}) \quad (1)$$

Manuscript received May 16, 1997; revised August 24, 1998. This work was supported by the National Science Council, R.O.C., under Grant NSC 87-2213-E-002-058.

The authors are with the Department of Electrical Engineering, National Taiwan University, Taipei, Taiwan, R.O.C. (e-mail: leonardo@emwave.ee.ntu.edu.tw; thc@emwave.ee.ntu.edu.tw).

Publisher Item Identifier S 0018-9480(99)00387-7.

where $\mathbf{p} = -2k\mathbf{i}_k = p\mathbf{i}_p$, $k = 2\pi f/c$, \mathbf{n} is an outward vector normal to the object surface $S(\mathbf{r})$, and the surface integral is over the illuminated portion of the object. By adding $\rho(\mathbf{p})$ with $\rho^*(-\mathbf{p})$ measured at the opposite side of the object and using the divergence theorem, one can obtain [1], [2]

$$\Gamma(\mathbf{p}) = \frac{2\sqrt{\pi}}{p^2} [\rho(\mathbf{p}) + \rho^*(-\mathbf{p})] = \int \gamma(\mathbf{r}) e^{-j\mathbf{p}\cdot\mathbf{r}} d\mathbf{r} \quad (2)$$

where $\gamma(\mathbf{r})$ is the characteristic function of the scattering object B , defined as

$$\gamma(\mathbf{r}) = \begin{cases} 1, & \mathbf{r} \text{ in } B \\ 0, & \mathbf{r} \text{ not in } B. \end{cases} \quad (3)$$

Equation (2) is known as the Bojarski's identity [1], [2]. It shows that an image of the scattering object B can be reconstructed from the backscattered far field measured at all frequencies and viewing angles through the Fourier inversion. The reconstructed image has a unity intensity inside the object according to (3).

In practice, (1) indicates that a line of $\rho(\mathbf{p})/p$ data recorded from one view by stepping the operating frequency in the microwave region is proportional to the one-dimensional discrete Fourier transformation of the projection image of object discontinuities on the illuminated surface along the observation direction \mathbf{i}_p [6]. Therefore, a set of one-dimensional projection images of the object scattering centers can be acquired from $\rho(\mathbf{p})/p$ data collected over a range of frequency and viewing angle. From the slice-projection theorem, a two-dimensional Fourier inversion of the Fourier domain data $\rho(\mathbf{p})/p$ then yields image of the specular points on the object illuminated surface. In a microwave diversity imaging measurement system [3], a VNA can be used to directly record the Fourier domain data (amplitude and phase) of the scattering object.

B. Six-Port Reflectometer and Calibration Method

Since the idea of six-port reflectometer was proposed in [4] and [5], it becomes an alternate approach to measure the complex ratio between two signals other than directly using a VNA. In a six-port reflectometer, the amplitude and phase of complex reflection coefficient is calculated from the measurement of power values at four output ports. The six-port reflectometer circuit is constructed using hybrids and detectors or power sensors, hence, its operation frequency range can be extended to the millimeter-wave region. However, the calibration procedure of a six-port reflectometer is much more complex than that of a VNA, and more computation efforts are required to calculate the desired reflection coefficient from the measured power values.

The calibration procedure basically consists of two steps. In the first step, the six-port reflectometer is transformed to an equivalent four-port reflectometer. This requires the determination of five parameters to characterize the six-port reflectometer [7]–[9]. The next step is to determine the six real (or three complex) parameters to characterize the equivalent four-port reflectometer [10]. To fulfill the requirements of these two calibration steps, we use a calibration circuit which consists of a variable attenuator and a variable phase shifter in our six-port microwave imaging system. The calibration data are taken for three different attenuation values and five phase-shift values. Note all these values are not required to be known. It will then result in a total of 15 sets of different input signals, which are sufficient for the step-one six-port to four-port calibration and the step-two four-port calibration.

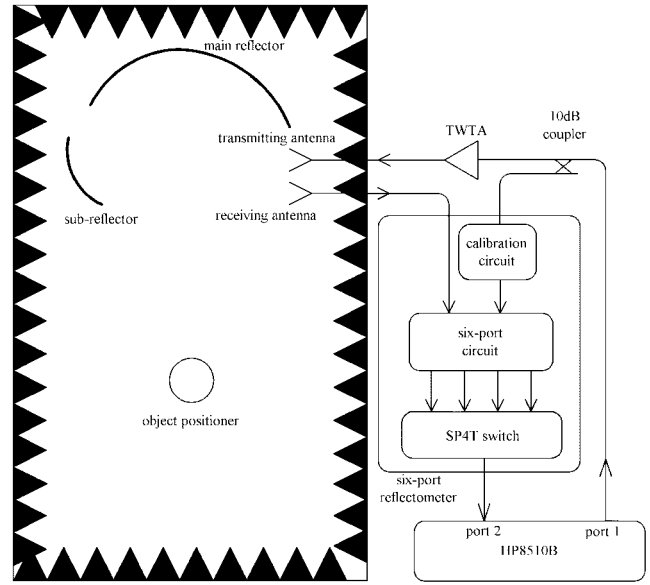


Fig. 1. Experiment arrangement of microwave diversity imaging system using six-port reflectometer with compact-range facility in an anechoic chamber.

III. EXPERIMENT ARRANGEMENT AND CALIBRATION PROCEDURE

A. Anechoic Chamber and Compact Range Arrangement

As shown in Fig. 1, the experiment arrangement has an anechoic chamber with a compact-range facility to provide a plane-wave illumination to the region of object positioner. The transmitting and receiving antennas are placed together with spacing about 15 cm as a backscattering arrangement. The main reflector and subreflector have the sizes about 2 and 0.9 m in diameter. In our measurement, the operation frequency is from 8 to 12 GHz.

In this arrangement, the transmitted signal from port 1 of an HP8510B is fed through a traveling-wave tube amplifier (TWTA) to the transmitting corrugated horn. A calibration circuit is connected to the coupled port of a 10-dB coupler to provide the reference signal to the six-port circuit. The received object scattered field from the receiving corrugated horn then goes to the other input port of six-port circuit. The four output ports of the six-port circuit are connected to an SP4T coaxial switch with its output port to port 2 of the HP8510B. The squared value of the S_{21} amplitude measured by an H8510B is then recorded to give the measurement of power values at each output port of a six-port circuit. The HP8510B, object positioner, and switch-control instrument are linked to a Sun Sparc-10 workstation through IEEE 488 interface.

B. Six-Port Reflectometer and Calibration Procedure

The six-port reflectometer contains a six-port circuit, calibration circuit, and SP4T coaxial switch. The six-port circuit consists of four 90° hybrids, as in [11]. The calibration circuit consists of an HP 8494H electronically controlled 0–11-dB stepped attenuator and a SEMFLEX MFR 60 637 coaxial line stretcher as a phase shifter.

In the calibration measurement, a metallic cylinder with diameter of 25.4 cm is placed on the object positioner, with the cylinder front edge at the center of positioner. A total of 15 sets of data are recorded by varying three attenuator step positions and five phase-shifter positions. Five parameters for characterizing the six-port reflectometer to four-port reflectometer transformation are firstly solved using the singular-value decomposition method. We then take one attenuator setting to be 0 dB, one associated phase shifter setting

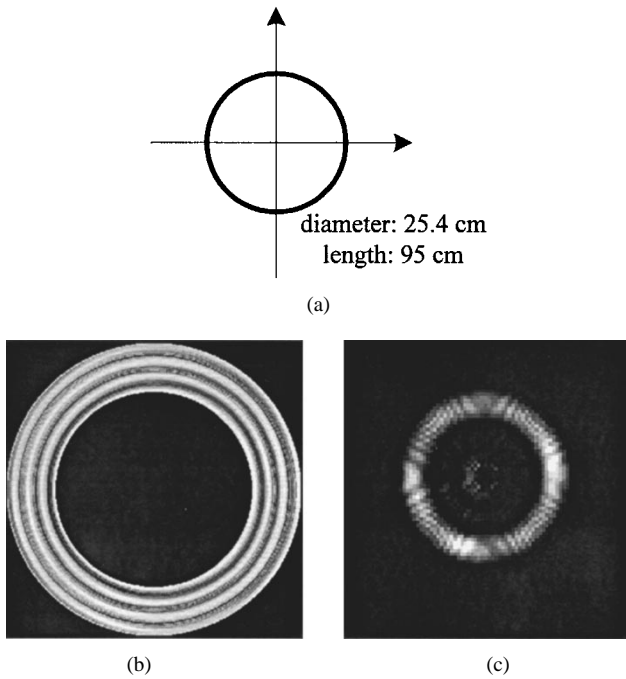


Fig. 2. Experiment results of a metallic cylinder with (a) scattering object, (b) Fourier domain data, and (c) reconstructed image.

to be 0° , and the measured reflection coefficient to be unity as the reference signal for the four-port reflectometer calibration. In this second-step calibration, three parameters are solved using ten sets from the previously recorded data, corresponding to two attenuator settings and five phase-shifter settings [10].

After the calibration, the calibration circuit is then set to its 0 dB and 0° setting for the microwave diversity imaging measurement, and the six-port measurement system becomes equivalent to a four-port (or VNA) measurement system. One can then use the same error model $S_m = S_c + S_t S_o S_r$ as that in a VNA scattering measurement system for anechoic chamber characterization. S_c is the clutter response of anechoic chamber. S_t and S_r are the responses for transmitting and receiving paths, including antennas and compact range. S_m and S_o are the measured and corrected object responses. Note in a microwave diversity imaging system S_c , S_t , and S_r are frequency responses only, whereas S_m and S_o are responses of frequency and view angle.

Let the response of the reference object before correction be $S_{\text{ref}}(f)$, and the measured response of the scattering object be $S_m(f, \theta)$. The corrected object response is then given by

$$S_o(f, \theta) = \frac{S_m(f, \theta) - S_c(f)}{S_{\text{ref}}(f) - S_c(f)} \quad (4)$$

where $S_c(f)$ is the room clutter. After recording the scattering object response in a polar format, a two-dimensional interpolation algorithm is used to transfer data into rectangular grids for two-dimensional fast Fourier transformation for image reconstruction.

IV. EXPERIMENT RESULTS

Experiment results of three different types of scattering objects, including a metallic cylinder, four distributed line scatterers, and a B-52 scaled aircraft model are presented. In all the measurements, the frequency used is stepped from 8 to 12 GHz for 101 points. The Fourier domain data and reconstructed image of a metallic cylinder are shown in Fig. 2. The cylinder diameter is 25.4 cm, and is placed at the center of the object positioner. The range of viewing angle is from

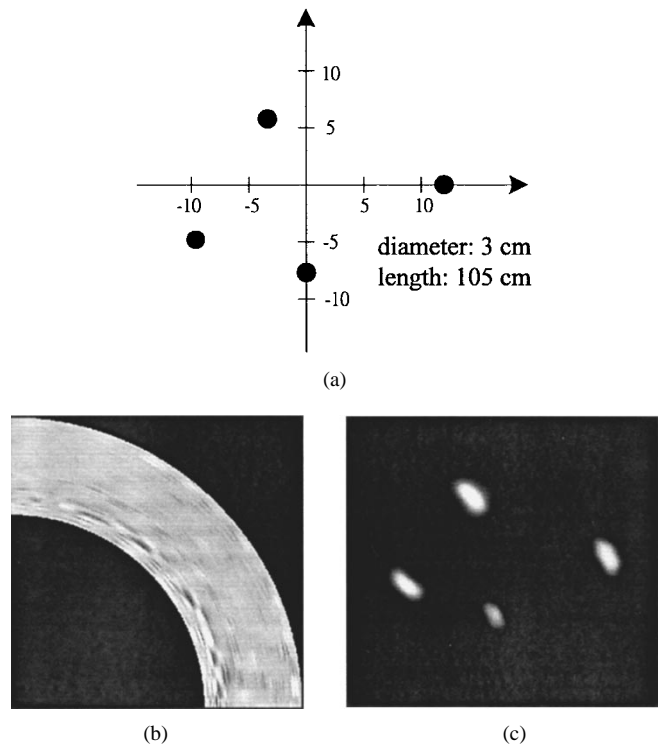


Fig. 3. Experiment results of four metallic line scatterers with (a) scattering objects, (b) Fourier domain data, and (c) reconstructed image.

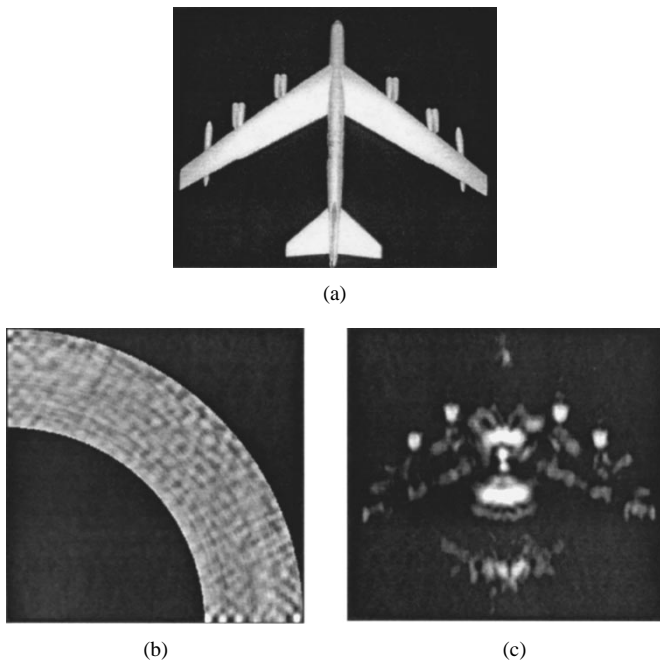


Fig. 4. Experiment results of a 72:1 scaled B-52 aircraft with (a) scattering objects, (b) Fourier domain data, and (c) reconstructed image.

0° to 360° for a total of 60 views. The reconstructed image given in Fig. 2(c) shows the shape of the cylinder with correct dimension.

Fig. 3 shows the results of four distributed line scatterers. The four line scatterers are placed at (12, 0), (0, -8), (-3.5, 6), and (-10, -5) in centimeters. The range of viewing angle is from 0° to 90° for 50 views. The reconstructed image gives the correct positions of four line scatterers.

Fig. 4 shows the results of a B-52 scaled aircraft model. The range of viewing angle is the same as that of four line scatterers. The

reconstructed image clearly shows the images of fuselage, wings, engines, and oil tanks. The bright circular shape image at the center area of fuselage is due to the supporting Styrofoam rod. It is worth noting that all the reconstructed microwave images are naturally edge enhanced because of the specular nature of microwave scattering from convex surfaces of the object under test.

V. CONCLUSION

Conventionally, the object scattered field for microwave diversity imaging is measured directly using a VNA. In this paper, we described the experiment arrangement and calibration procedure using a six-port reflectometer developed in our compact-range facility. The reconstructed images show the same quality as those using VNA's. These results indicate that with the use of a six-port reflectometer, one can reduce the cost of microwave diversity image facility and also extend the operation frequency to the millimeter-wave range.

REFERENCES

- [1] R. M. Lewis, "Physical optics inverse diffraction," *IEEE Trans. Antennas Propagat.*, vol. AP-24, pp. 308–314, May 1969.
- [2] N. N. Bojarski, "A survey of physical optics inverse scattering identity," *IEEE Trans. Antennas Propagat.*, vol. AP-30, pp. 980–989, Sept. 1982.
- [3] N. H. Farhat, "Microwave diversity imaging and automated target identification based on models of neural networks," *Proc. IEEE.*, vol. 77, pp. 670–680, May 1989.
- [4] C. A. Hoer, "The six-port coupler: A new approach to measuring voltage, current, power, impedance, and phase," *IEEE Trans. Instrum. Meas.*, vol. IM-21, pp. 466–470, Nov. 1972.
- [5] G. F. Engen, "A (historical) review of the six-port measurement technique," *IEEE Trans. Microwave Theory Tech.*, vol. 45, pp. 2414–2417, Dec. 1997.
- [6] T. H. Chu and D. B. Lin, "On microwave imagery using Bojarski's identity," *IEEE Trans. Microwave Theory Tech.*, vol. 37, pp. 1141–1144, July 1989.
- [7] G. F. Engen, "Calibration of an arbitrary six-port junction for measurement of active and passive circuit parameters," *IEEE Trans. Instrum. Meas.*, vol. IM-22, pp. 295–299, Dec. 1973.
- [8] —, "Calibrating the six-port reflectometer by means of sliding terminations," *IEEE Trans. Microwave Theory Tech.*, vol. MTT-26, pp. 951–957, Dec. 1978.
- [9] G. F. Engen and C. A. Hoer, "'Thru-reflect-line': An improved technique for calibrating the dual six-port automatic network analyzer," *IEEE Trans. Microwave Theory Tech.*, vol. MTT-27, pp. 987–993, Dec. 1979.
- [10] I. Kása, "Closed-form mathematical solutions to some network analyzer calibration equations," *IEEE Trans. Instrum. Meas.*, vol. IM-23, pp. 399–402, Dec. 1974.
- [11] G. F. Engen, "An improved circuit for implementing the six-port technique of microwave measurement," *IEEE Trans. Microwave Theory Tech.*, vol. MTT-27, pp. 847–853, Oct. 1979.

Bandwidth and Dispersion Characteristics of a New Rectangular Waveguide with Two L-Shaped Septa

Pradip Kumar Saha and Debatosh Guha

Abstract—A new rectangular waveguide with two L-shaped septa has been added to the family of septa-loaded broad-band waveguides. Its modal characteristics and dispersion in inhomogeneously loaded version have been theoretically determined. The cutoff frequency and the bandwidth of the lowest TE mode are also compared with the experimentally measured values obtained with a test cavity.

Index Terms—Broad-band waveguide, septum waveguide.

I. INTRODUCTION

In recent years, this paper's authors have been experimenting, albeit theoretically, with rectangular waveguides of unusual cross section (which can be potential alternatives for ridged waveguides), the celebrated broad-band transmission media. The first structure proposed in [1]–[3] contained T-shaped metal septa in place of solid ridges, as shown in Fig. 1(a) and (b). This prompted a few other works, including experimental verification of modal cutoff [4]–[8]. On the application side, an evanescent-mode filter employing T-septa waveguide has been reported [9]. Since the idea is to introduce a parallel-plate region with suitable metallic loading in a rectangular waveguide where a TEM-like field can exist, a variant of the double T-septa guide (DTSG) was proposed, in which the T-septa were replaced by L-shaped septa, as shown in Fig. 1(c) and (d) [10], [11]. These double L-septa guides, designated as DLSG1 and DLSG2 in [10], obviously would be more difficult to fabricate than the ridged waveguides, but promise attractive cutoff and bandwidth characteristics of the dominant mode.

The continued search for potential broad-band waveguides has resulted in a proposal for yet another septa guide [12], a variant of DLSG2, in which the two L-septa are mounted in a different configuration, as shown in Fig. 2(a). This little variation in geometry has caused appreciable modification in modal characteristics. The new waveguide will be referred to as DLSG3. A generalized inhomogeneous DLSG3 [Fig. 2(b)] is considered for hybrid-mode analysis. Theoretical dispersion characteristics of the HE-type hybrid modes and theoretical cutoff and bandwidth characteristics of the dominant modes of air-filled and inhomogeneous (septa-gap-filled) DLSG3 are presented together with some comparison with other septa guides.

The cutoff frequency of the dominant mode was also experimentally determined from the resonant frequency measurement on a cavity made of DLSG3. The experimental value of the cutoff frequency of the test waveguide is compared with the theoretically computed value.

Although the results presented here relate to hybrid modes, backward-wave and complex modes can also exist in inhomogeneous (particularly the gap-filled type) T- and L-septa guides under the condition of thick dielectric slab and high dielectric constant. These

Manuscript received May 27, 1997; revised April 29, 1998. This work was supported by the Centre of Advanced Studies in Radio Physics and Electronics, University of Calcutta, Calcutta, India.

The authors are with the Institute of Radio Physics and Electronics, University Colleges of Science and Technology, University of Calcutta, Calcutta-700 009, India (e-mail: dguha@cucc.ernet.in).

Publisher Item Identifier S 0018-9480(99)00388-9.